Technical Report: In-situ calibration of six-axis force/torque transducers on legged robot

Ziyou Wu, and Shai Revzen

***Abstract*— In this paper, we present a calibration procedure for simultaneously measuring all foot contact wrenches (forces and torques) of a multi-legged robot using 6-DoF load cells installed at the hips.**

I. Introduction

Force/torque(f/t) transducers are commonly used in robotics applications to sense the interaction between robots and their environment [1]. For example, f/t transducers are used in robotics surgery [2], manipulation [3], [4], robot locomotion [5]–[7], etc. Knowing contact forces allows robots to sense its surrounding environments, and enables better planning and control through feedback. Specifically, legged robots usually move around with making and breaking contacts with the ground; f/t transducers can measure how the load is distributed among legs, how much propulsion each leg gives, and therefore facilitate the study in modeling and control of legged mechanisms. They can be used in contact detection [5], gait modeling [6], state estimation [8], terrain classification [7], maintaining stability [9], etc.

We are interested in simultaneously measuring the ground reaction force on each individual foot of multi-legged robots with low degree of freedom (DoF) legs [10], [11], especailly, the robot family inspired from rapid running cockroaches [12], [13]. Masses of such robots are mainly concentrated at the bodies, allowing fast swinging of the legs. Our previous experiments showed that slipping was an essential part in modeling those robots, especially when a robot steered [14]. The body velocity with slipping was easily modeled in a data-driven form, where body velocity was linearly dependent on body shape change rate [15]. Although the model was seemingly aligned with a viscous friction model instead of Coulomb, the robot interacted with ground through dry contacts with sliding. Hence, we want to measure the actual contact forces when robot slips to understand why that model worked.

We installed each leg with one f/t transducer at the hip of the hexapod used in aforementioned previous experiments, enabling us to measure the wrench (forces and torque) interacting between leg and robot chassis. The transducer installation point was chosen at the hip, in order to maintain the lightweight, fast-swinging nature of the legs. In addition, we found the commercial transducers were usually heavy and fragile to impacts, and hence infeasible to attach them directly at the tip of a foot. The wrenches applied to the transducer became the ground reaction wrenches coupled together with the wrench that resulted from leg gravity. As such, the applied wrench must be decoupled, in order to isolate the ground reaction wrench we seek.

Few have measured multi-legged ground reaction wrenches simultaneously at each individual foot. One example is in [16], wherein, the authors measured 3D ground reaction forces for a hexapod Rhex. The authors did not provide details on characterization and analysis of measurement error, but did provide 2N as the maximum error. The authors of [17] performed in-situ calibration with f/t transducers mounted on the shoulders, hips and feet of a bipedal robot. They used the model from their design file to extract the center of mass (CoM) of each segment and estimate the torque resulted from the gravity of each segment. However, the discrepancy between actual and designed CoM caused error in the torque measurement.

In this paper, we present a calibration procedure enabling simultaneous measurement of all foot contact wrenches of a multi-legged robot using 6-DoF f/t transducers installed at the hips. We start with introducing the experimental setup in §I-A, followed by difficulties we met when using the transducers naively according to the manufacturer's guide in §I-B. We present the problem statement including notations and f/t measurement model in this calibration work in §II, followed by our calibration method in §III. We then show the calibration results in §IV and end with discussions in §V.

A. Experimental system: robot and sensors

We used pre-existing hexapedal design with 1-DoF legs, BigAnt [11], [18], [19] (figure 1). The measurement goal of our experiment was to estimate ground reaction wrenches relative to a "floating base" frame – origin at robot CoM of a reference body shape. Wherein, the axes were aligned with -z for gravity, and the xz plane is the mirror plane for left-right body symmetry. In other words, it was the world frame with $x-$axis always aligned with robot heading, and origin centered at robot CoM. The robot gait was simply governed by a clock-driven, open-loop tripod gait, composed of a fast swinging phase, and a slow touch-down phase [10]. The same robot was used in previous studies, where the authors showed the robot

Z. Wu is with Robotics department in University of Michigan, Ann Arbor, MI 48105, USA (email: wuziyou@umich.edu).

S. Revzen is with Electrical and Computer Engineering, Ecology and Evolutionary Biology, Applied Physics and Robotics department in University of Michigan, Ann Arbor, MI 48105, USA (email: shrevzen@umich.edu).

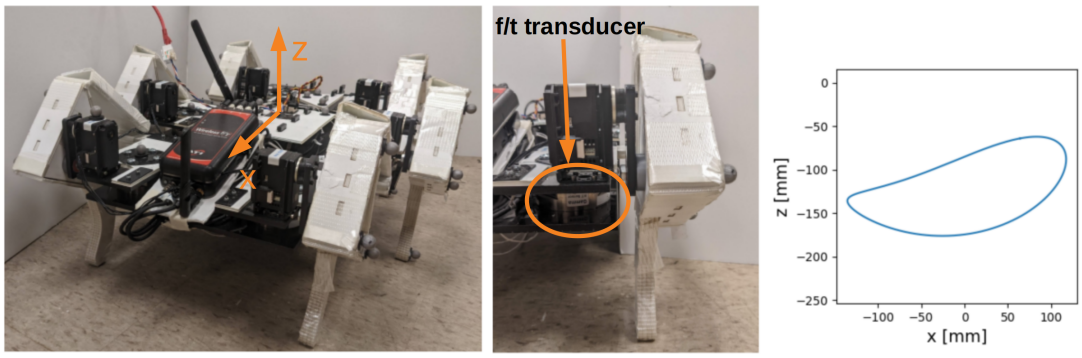

Fig. 1: BigAnt equipped with six 6-axis force/torque transducers (left). Zoomed-in view of one leg with f/t transducers (middle). 1-DoF toe tip trajectory in robot body frame xz-plane (right).

must slip during turning due to the constraints imposed by its 1-DoF legs [14] and the body velocity with slipping could be modeled through a simple data-driven principally kinematic form [15].

On the BigAnt robot, each leg was driven by a four bar mechanism, manufacuted using PARF (plate and reinforced flexure) technique [11]. The CoM of each leg moved as a function of the motor shaft angle of that respective leg, and hence, the torque resulted by the gravity of a leg was a function of its shaft angle. Underneath each leg, we installed an ATI Net Force/Torque Gamma transducer, measuring all six components of force and torque at 100Hz. The robot chassis was manufactured using 1/4 inch Acrylonitrile butadiene styrene (ABS) board. Each leg was actuated by a servo motor (Robotis Dynamixel MX106). All Dynamixels were daisy chained and communicated over RS-485 serial interface. The total weight of the robot was 8.18kg, measured by a digital hanging scale. Along with F/T data, we also recorded robot kinematic data using the reflective marker motion tracking system (10 Qualisys Oqus-310+ cameras at 100 fps, 12 markers on the chassis and 4 markers per leg).

B. Pre-experimental f/t transducer measurement validations

In our work, we have encountered great difficulty in getting accurate ground reaction forces measurement. As a sanity check, we collected measurements with the robot stand statically at different poses. At this phase of the research, we naively used f/t transducers following the user manual [20], where we used the transducer reading with all feet in the air as the constant bias term, and then subtracted that bias from all measurements. However, using this method, the measurement results failed our sanity check. When robot standing at different poses, the sum of all ground contact wrenches transformed to the floating base frame was far from equal to robot gravity with zero torque.

We collected f/t measurements and motion tracking data with BigAnt standing at different poses. Each leg had three phase choices: the shaft angle at 0^o(pointing straight down) or $\pm 36^o$. In total, there were $3^6 = 729$ different standing poses. During the experiment, we waited for 5 seconds

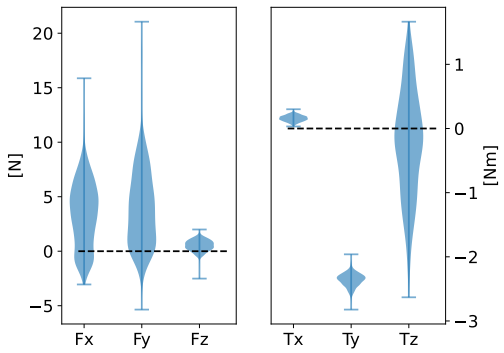

Fig. 2: Violin plot of the sum of all wrenches acting on the robot when standing at different poses, with f/t transducers calibrated with naive offset removal.

between two different poses. When a pose transited to the next, we observed that both the wrench and motion tracking measurements exhibited an overshooting oscillatory behavior. We estimated the 1st order derivative of both data streams using a 2nd order `scipy.signal.savgol_filter` filter. A pose was considered to reach steady state, if the L2-norm of numerical differentiation on force data decayed to less than 1N/s. If a pose stayed at steady state for more than 1.5s, we took the median of the steady state measurements to represent this pose. Otherwise, we discarded that pose. After this process, there were 635 poses left. We further discarded the poses that did not have all 12 markers on the chassis being tracked by motion capture system. In the end, we had $P = 543$ poses. We transformed the transducer measurements from transducer frame into the floating base frame, where frame transformations were estimated through motion tracking data. When the robot stood still, the sum of all wrenches acting on the robot was expected to be zero. However, we observed the sum of planar forces had 5N standard deviation, and the force was distributed from -5N to 20N, shown in figure 2.

The transducers themselves were pre-calibrated by the ATI company, and carefully used in their normal operating region. We believed the main error source was the miscalibration after

the transducers installed onto the robot. This miscalibration is in fact common among all kind of robots, including legged robots and manipulators, using f/t transducers.

C. Previous f/t transducer calibration works

Manufacturers have recognized an offset error on f/t transducers, i.e. nonzero reading showed up even the transducer bore no load. They usually recommend people to take all transducers out, and re-calibrate them once a while. This calibration could remove the transducer offset, but will be unable to account for the gravity of the legs. In addition, removal the transducers could also result in a different assembling error every time. Hence, we decided to do the calibration in-situ.

Many previous works on manipulators with f/t transducers attached to the tool-tips have recognized errors in f/t sensing. A common method to perform in-situ calibration on some parameter of interest, is to attach a standard mass or a tool with fixed mass to the transducer, and then take several measurements with transducer at different orientations. Using the fact that the external force applied to transducer, the gravity of the attached mass, is fixed in the world frame, one can use least square methods to estimate calibration parameters. The authors of [3], [21] solved for a in-situ calibration matrix which transformed strain gauge values to forces and torques. The authors of [22] solved for in-situ calibration matrix together with a rotation matrix between world frame and the robot base frame, to account for the error caused by a tilted robot base of a manipulator. The authors of [23] did gravity compensation for the tool together with estimating the transformation matrix between transducer frame and the robot frame. All of the aforementioned works attached their f/t transducer relatively fixed with respect to the end effector.

D. Challenges

On our experimental setup, we met other difficulties not being addressed by previous calibration works. Manipulators usually had tools relatively fixed attached to f/t transducers. In contrast, the CoM of each leg was not constant in body frame, but instead varying upon its shaft angle. We also observed the placement of the transducers were not perfect relative to robot body frame, having mounting position and orientation errors. The origin of the robot frame (the geometric center of the robot) was also not the same as CoM of the robot. It was hard to estimate the CoM of a robot built and assembled with parts using many kinds of materials. During in-situ calibration on a manipulator, the orientation of f/t transducer could be almost perfectly positioned by controlling its joints, whereas we needed to hang the robot in opposite directions to change the transducer frame orientation. It was difficult to accurately measure the hanging angle of each transducer on the whole robot body together with mounting orientation error. In this paper, we tried to design a calibration framework to characterize the aforementioned errors.

Besides those errors, we also found the transducer casing was not well-sealed. With zero load on the sensor, wrapped around the sensor case with 1-7 rubber bands (OfficeMax size 16), the forces in transducer xy axis changed 1N in the reading. By gently pulling one rubber band to create a non-uniform load around the case, the forces in transducer xy axis changed 3N.

II. Force/torque sensing model

In this section, we present the notations, sensing error model and calibration parameters.

A. Notations

We use bold upper-case letters to represent matrices (e.g. $\mathbf{T}, \mathbf{R}$); and bold lower-case letters to represent vectors (e.g. $\mathbf{w}, \mathbf{r}$). We use the generalized force, wrench $\mathbf{w} = [\mathbf{f}; \boldsymbol{\tau}]^T$, to represent linear components (forces $\mathbf{f} \in \mathbb{R}^3$) and angular components (torques $\boldsymbol{\tau} \in \mathbb{R}^3$). We use ; to separate elements in a column vector. We use $\mathbf{T}_{\mathsf{A}}^{\mathsf{B}}$ to represent rigid-body motion $\mathbf{SE}(\mathbf{3})$ from frame A to frame B. The homogeneous transformation representation is:

$$\mathbf{T}_{\mathsf{A}}^{\mathsf{B}} = \begin{bmatrix} \mathbf{R}_{\mathsf{A}}^{\mathsf{B}} & \mathbf{p}_{\mathsf{A}}^{\mathsf{B}} \\ \mathbf{0} & 1 \end{bmatrix} \in \mathbb{R}^{4\times 4}$$

Here $\mathbf{R}_{\mathsf{A}}^{\mathsf{B}} \in SO(3)$ is the rotation from frame A to B, and $\mathbf{p}_{\mathsf{A}}^{\mathsf{B}} \in \mathbb{R}^3$ is the translation from the origin of A to the origin of B. With an abuse of notation, we omit 1 in the homogeneous transformation in the later calculations, i.e. $\mathbf{r}^{\mathsf{A}} \in \mathbb{R}^3$, $\mathbf{T}_{\mathsf{A}}^{\mathsf{B}}\mathbf{r}^{\mathsf{A}} := \mathbf{T}_{\mathsf{A}}^{\mathsf{B}}[\mathbf{r}^{\mathsf{A}}; 1] = [\mathbf{r}^{\mathsf{B}}; 1] =: \mathbf{r}^{\mathsf{B}}$. We transform wrenches from frame A to frame B via the transposed adjoint representation of transformation $\mathbf{T}_{\mathsf{B}}^{\mathsf{A}}$:

$$\mathbf{w}^{\mathsf{B}} = [\mathsf{Ad}_{\mathbf{T}_{\mathsf{B}}^{\mathsf{A}}}]^T \mathbf{w}^{\mathsf{A}}$$

$$\begin{bmatrix} \mathbf{f}^{\mathsf{B}} \\ \boldsymbol{\tau}^{\mathsf{B}} \end{bmatrix} = \begin{bmatrix} (\mathbf{R}_{\mathsf{B}}^{\mathsf{A}})^T & \mathbf{0} \\ -(\mathbf{R}_{\mathsf{B}}^{\mathsf{A}})^T \left[\mathbf{p}_{\mathsf{B}}^{\mathsf{A}}\right] & (\mathbf{R}_{\mathsf{B}}^{\mathsf{A}})^T \end{bmatrix} \begin{bmatrix} \mathbf{f}^{\mathsf{A}} \\ \boldsymbol{\tau}^{\mathsf{A}} \end{bmatrix}$$

where the bracket $\left[\mathbf{p}_{\mathsf{A}}^{\mathsf{B}}\right]$ lifts the 3d vector $\mathbf{p}_{\mathsf{A}}^{\mathsf{B}}$ to a skew symmetric matrix. The frame of reference for a value of interest is on its upper right corner. We use k to denote the index of the legs, i.e. wrench w.r.t. frame A on leg k is $\mathbf{w}_{\mathsf{k}}^{\mathsf{A}}$.

The coordinate frames of interests are B: robot body frame; C: robot body frame with centered at CoM; W: floating base frame; ft_{k}: f/t transducer frame of the k^{th} leg. We use $\mathbf{g} = [0, 0, g]$ to represent the gravitational acceleration in the floating base frame.

We use ϕ to represent the shaft angle governing the shape of four-bar linkage leg, m to represent the mass of a leg, and $\mathbf{r}(\phi)$ to represent the leg CoM as a function of ϕ. We use $i = 1, \cdots, N$ to denote index for time series. We use $\square^*$ to denote the optimal value for the variable in optimization. In §III-A, where we do the hanging experiment to estimate transducer and leg gravity offsets, we use $\square^{\downarrow}$ and $\square^{\uparrow}$ to denote a value associated with positive and negative hanging direction. We use $\square^- =: (\square^{\downarrow} - \square^{\uparrow})/2$ and $\square^+ =: (\square^{\downarrow} + \square^{\uparrow})/2$ to denote subtraction and addition of some value measured in two opposite hanging directions.

B. Sensing model

From our experiments, we noticed that for each transducer there existed a constant offset, independent of load, which was also mentioned in ATI f/t transducer manual [20]. We modeled the measured wrench $\mathbf{w}_m^{\mathsf{ft}_{\mathsf{k}}}$ by the k^{th} force/torque transducer,

as the sum of the applied wrench $\mathbf{w}_a^{\text{ft}_\text{k}}$, an unknown transducer offset $\mathbf{w}_o^{\text{ft}_\text{k}} \in \mathbb{R}^6$ and random noise $\mathbf{n}$,

$$\mathbf{w}_m^{\text{ft}_\text{k}} =: \mathbf{w}_a^{\text{ft}_\text{k}} + \mathbf{w}_o^{\text{ft}_\text{k}} + \mathbf{n} \tag{1}$$

Since the transducers were installed underneath the legs, when a leg was in swinging phase (not contacting the ground), the wrench resulted from the leg gravity was applied to the transducer. We decomposed the applied wrench $\mathbf{w}_a^{\text{ft}_\text{k}}$ into two parts: the wrench resulted from the gravity of k^{th} leg and the ground contact wrench. The shaft angle ϕ_k governed the shape of four-bar linkage of each leg, and hence changed its CoM. We modeled the k^{th} leg CoM position in transducer frame by $\mathbf{r}_\text{k}^{\text{ft}_\text{k}}(\phi_\text{k})$. We used leg gravitational offset $\mathbf{w}_{\text{leg,k}}^{\text{W}}(\phi_\text{k})$, a function of ϕ_k, to model its gravity, and the torque generated by gravity. The gravitational acceleration is constant in the floating base frame. We transformed leg CoM position in the transducer frame to the floating base frame, and leg gravitational offset wrench:

$$\mathbf{w}_{\text{leg,k}}^{\text{W}}(\phi_\text{k}) =: [m_k\mathbf{g}; \mathbf{T}_{\text{ft}_\text{k}}^{\text{W}}\mathbf{r}_\text{k}^{\text{ft}_\text{k}}(\phi_\text{k}) \times m_k\mathbf{g}]$$

We decomposed the transformation from the k^{th} f/t transducer to floating base frame in four steps:

$$\mathbf{T}_{\text{ft}_\text{k}}^{\text{W}} =: \mathbf{T}_{\text{C}}^{\text{W}}\mathbf{T}_{\text{ft}_\text{k}}^{\text{C}} = \mathbf{T}_{\text{C}}^{\text{W}}\mathbf{T}_{\text{B}}^{\text{C}}\tilde{\mathbf{T}}_k\mathbf{T}_{\text{ft}_\text{k}}^{\text{B}} \tag{2}$$

1. a nominal transformation, $\mathbf{T}_{\text{ft}_\text{k}}^{\text{B}}$, from the k^{th} transducer frame to body frame, calculated from robot design files;
2. unknown transformation $\tilde{\mathbf{T}}_k$ to compensate the installation or manufacturing error, which was not captured by step 1;
3. unknown translation $\mathbf{T}_{\text{B}}^{\text{C}}$ between the origin of the body frame and robot CoM.
4. a pure rotation $\mathbf{T}_{\text{C}}^{\text{W}}$ estimated from markers measured by motion tracking system, rotating the body frame centered at CoM into floating base frame.

Let $\mathbf{g}^{\text{C}} = \mathbf{R}_{\text{W}}^{\text{C}}\mathbf{g}$ be the gravitational acceleration rotated into body CoM frame. We used $\mathbf{w}_{\text{gc},k}^{\text{C}}(\phi_\text{k})$ to denote the ground contact wrench in the body CoM frame, calculated from the applied wrench $\mathbf{w}_a^{\text{ft}_\text{k}}$ transformed in the CoM frame and subtracted by the wrench from leg gravity.

$$\begin{aligned}
\mathbf{w}_{\text{gc},k}^{\text{C}}(\phi_\text{k}, \mathbf{g}^{\text{C}}) &=: [\text{Ad}_{(\mathbf{T}_{\text{ft}_\text{k}}^{\text{C}})^{-1}}]^T\mathbf{w}_a^{\text{ft}_\text{k}} - \mathbf{w}_{\text{leg,k}}^{\text{C}}(\phi_\text{k}, \mathbf{g}^{\text{C}}) \\
\text{(substitute } \mathbf{T}_{\text{C}}^{\text{ft}_\text{k}} \text{ by eqn.2)} &= [\text{Ad}_{(\mathbf{T}_{\text{B}}^{\text{C}}\tilde{\mathbf{T}}_k\mathbf{T}_{\text{ft}_\text{k}}^{\text{B}})^{-1}}]^T\mathbf{w}_a^{\text{ft}_\text{k}} - \mathbf{w}_{\text{leg,k}}^{\text{C}}(\phi_\text{k}, \mathbf{g}^{\text{C}}) \\
\text{(substitute } \mathbf{w}_a^{\text{ft}_\text{k}} \text{ by eqn.1)} &= [\text{Ad}_{(\mathbf{T}_{\text{B}}^{\text{C}}\tilde{\mathbf{T}}_k\mathbf{T}_{\text{ft}_\text{k}}^{\text{B}})^{-1}}]^T(\mathbf{w}_m^{\text{ft}_\text{k}} - \mathbf{w}_o^{\text{ft}_\text{k}}) \\
\text{(rewrite } \mathbf{w}_o^{\text{ft}_\text{k}} \text{ in f/t elements)} &\quad - [m_k\mathbf{g}^{\text{C}}; \mathbf{T}_{\text{B}}^{\text{C}}\tilde{\mathbf{T}}_k\mathbf{T}_{\text{ft}_\text{k}}^{\text{B}}\mathbf{r}_\text{k}^{\text{ft}_\text{k}}(\phi_\text{k}) \times m_k\mathbf{g}^{\text{C}}]
\end{aligned} \tag{3}$$

It could be transformed into the floating base frame simply by the motion tracking rotation $[\text{Ad}_{\mathbf{T}_{\text{W}}^{\text{C}}}]^T$. All the unknown calibration parameters were highlighted in eqn. 3. In the rest of the paper, leg CoM $\mathbf{r}_\text{k}(\phi_\text{k})$ was always considered to be in the transducer ft_k frame, associated with the k^{th} shaft angle, so we omitted ft_k the leg CoM and k in ϕ_k, as $\mathbf{r}_\text{k}(\phi)$ to simplify the notation.

III. Calibration Method

In this section, we showed our method to infer those unknown calibration parameters through several optimizations with measurement data. The optimization goal function was formulated using the fact that the gravity of the robot and its legs was constant in the floating base frame. Our calibration had two steps: (1) we estimated the transducer offset $\mathbf{w}_o^{\text{ft}_\text{k}}$ and leg gravity offset $\mathbf{w}_{\text{leg,k}}^{\text{W}}$, by summing up the measurements with leg gravity acting in opposite directions in the transducer frame. Perfectly opposite measurements were never possible in reality. A small rotational term could leak m_kg into the other two directions, and polluted the estimation of offsets. We considered a small infinitesimal skew symmetric matrix as rotation error, and solved that together with the offsets. (2) we estimated the transformation error together with the unknown translation between body frame origin and CoM $\mathbf{T}_{\text{B}}^{\text{C}}\tilde{\mathbf{T}}_k$, by having the robot standing at different poses, then optimizing the error between the sum of all ground contact wrenches in floating frame and $[0, 0, G_{\text{robot}}, 0, 0, 0]^T$, namely the robot gravity with zero total torque.

A. Transducer offset and leg gravity offset

In the first step, we estimated the leg gravity, leg CoM as a function of its shaft angle, and transducer offset through measurements taken from the robot hanging (zero ground contact wrenches) in opposite directions with slowly (quasi-static) rotating their legs in ten full cycles. We showed BigAnt robot hanging in opposite z-direction in figure 3. The torque that resulted from leg gravity involved a cross-product with leg CoM, which left a one-dimension null space when estimating from one pair of hanging experiment (more details in §III-A.3). To get full dimensional CoM estimation, we did the experiment in two pairs of opposite orientations, transducer $\pm x$-axis, $\pm z$-axis aligning with gravity. In the rest of this section, we used the experiments of transducer $\pm x$-axis aligning with gravity to explain the calculation. The calculation with z-axis positive or negative direction aligning with gravity could be performed in analogy.

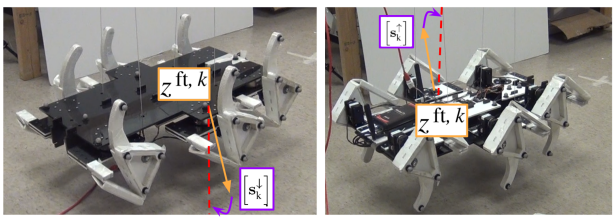

Fig. 3: BigAnt robot hanging with transducer z-aixs positive z^{ft_k} (orange) and negative direction aligning with gravity direction (red); $\left[\mathbf{s}_\text{k}^{\downarrow}\right]$ and $\left[\mathbf{s}_\text{k}^{\uparrow}\right]$ (purple): skew symmetric matrices modeling the hanging orientation error.

1) Hanging measurement model: We considered a measurement model using a skew symmetric matrix $[\mathbf{s}_\text{k}]$, lifted from $\mathbf{s}_\text{k} \in \mathbb{R}^3$, to model the axes misalignment error between the direction of gravity and the transducer axis. We assumed $\mathbf{s}_\text{k}$ was constant throughout one time series, i.e. the transducer orientation did not change throughout the measurement. The

skew symmetric matrix $[\mathbf{s}_\mathrm{k}]$, the tangent space at identity rotation, could be viewed as an infinitesimally small rotation. The applied wrench, when leg gravity aligning with positive x-axis of the transducer frame, became

$$\mathbf{f}_a^{\mathrm{ft_k},\downarrow} = (\left[\mathbf{s}_\mathrm{k}^{\downarrow}\right] + \mathbf{I}) m_k \mathbf{g}_x;\ \boldsymbol{\tau}_a^{\mathrm{ft_k},\downarrow} = [\mathbf{r}_\mathrm{k}(\phi)]\,(\left[\mathbf{s}_\mathrm{k}^{\downarrow}\right] + \mathbf{I}) m_\mathrm{k} \mathbf{g}_x$$

Its opposite applied wrench, when leg gravity aligning with negative x-axis of the transducer frame, was the same magnitude with opposite direction.

$$\mathbf{f}_a^{\mathrm{ft_k},\uparrow} = -(\left[\mathbf{s}_\mathrm{k}^{\uparrow}\right] + \mathbf{I}) m_k \mathbf{g}_x;\ \boldsymbol{\tau}_a^{\mathrm{ft_k},\uparrow} = -\,[\mathbf{r}_\mathrm{k}(\phi)]\,(\left[\mathbf{s}_\mathrm{k}^{\uparrow}\right] + \mathbf{I}) m_k \mathbf{g}_x$$

Here $\left[\mathbf{s}_\mathrm{k}^{\downarrow}\right]$ and $\left[\mathbf{s}_\mathrm{k}^{\uparrow}\right]$ were two skew symmetric matrices, accounting for two different small rotations between f/t transducer positive or negative x-axis and world z-axis. During the experiment, we measured f/t data for both of these two configurations, with the same set of varying shaft angles ϕ_i, for $i = 1, \cdots, N$, covering the full range of motion multiple times. We modeled the measured wrenches, according to eqn. 1, and partitioned them into their force and torque components in eqn. 4-7, where $\boldsymbol{\nu}_i^{\downarrow}, \boldsymbol{\nu}_i^{\uparrow}, \boldsymbol{\omega}_i^{\downarrow}, \boldsymbol{\omega}_i^{\uparrow}$ were realization of random noise for the i^{th} measurement.

$$\mathbf{f}_{m,i}^{\mathrm{ft_k},\downarrow} = (\left[\mathbf{s}_\mathrm{k}^{\downarrow}\right] + \mathbf{I}) m_\mathrm{k} \mathbf{g}_x + \mathbf{f}_o^{\mathrm{ft_k}} + \boldsymbol{\nu}_i^{\downarrow} \tag{4}$$

$$\mathbf{f}_{m,i}^{\mathrm{ft_k},\uparrow} = -(\left[\mathbf{s}_\mathrm{k}^{\uparrow}\right] + \mathbf{I}) m_k \mathbf{g}_x + \mathbf{f}_o^{\mathrm{ft_k}} + \boldsymbol{\nu}_i^{\uparrow} \tag{5}$$

$$\boldsymbol{\tau}_{m,i}^{\mathrm{ft_k},\downarrow} = [\mathbf{r}_\mathrm{k}(\phi_i)]\,(\left[\mathbf{s}_\mathrm{k}^{\downarrow}\right] + \mathbf{I}) m_\mathrm{k} \mathbf{g}_x + \boldsymbol{\tau}_o^{\mathrm{ft_k}} + \boldsymbol{\omega}_i^{\downarrow} \tag{6}$$

$$\boldsymbol{\tau}_{m,i}^{\mathrm{ft_k},\uparrow} = -\,[\mathbf{r}_\mathrm{k}(\phi_i)]\,(\left[\mathbf{s}_\mathrm{k}^{\uparrow}\right] + \mathbf{I}) m_\mathrm{k} \mathbf{g}_x + \boldsymbol{\tau}_o^{\mathrm{ft_k}} + \boldsymbol{\omega}_i^{\uparrow} \tag{7}$$

2) Leg gravity, $\mathrm{m_k g}$*:* We subtracted two opposite force measurements between eqn. 4 and eqn. 5. By dividing the difference by 2, we got the leg gravity multiplied by a small rotation error term in the front.

$$\frac{(4)-(5)}{2}: \quad \mathbf{f}_{m,i}^{\mathrm{ft_k},-} = \left(\frac{\left[\mathbf{s}_\mathrm{k}^{\downarrow}\right] + \left[\mathbf{s}_\mathrm{k}^{\uparrow}\right]}{2} + \mathbf{I}\right) m_\mathrm{k} \mathbf{g}_x + \frac{\boldsymbol{\nu}_i^{\downarrow} - \boldsymbol{\nu}_i^{\uparrow}}{2}$$

The sum of two skew symmetric matrices is still skew symmetric, denoted by $\left[\mathbf{s}_\mathrm{k}^{+}\right] = (\left[\mathbf{s}_k^{\downarrow}\right] + \left[\mathbf{s}_k^{\uparrow}\right])/2$. Ideally, $m_\mathrm{k}\mathbf{g}_x$ was equal to $[m_\mathrm{k} g, 0, 0]$, a constant value in x component, and zeros in y, z components. Taking that as the optimization goal, with N measurement samples $\mathbf{f}_{m,i}^{\mathrm{ft_k},-}$ for $i = 1, \ldots, N$, we solved for $\mathbf{s}_\mathrm{k}^{+}$ using `scipy.optimize.least_squares` with the Trust Region Reflective algorithm and cost function tolerance 10^{-3}.

$$\mathbf{s}_\mathrm{k}^{+,*} = \arg\min_{\mathbf{s}_\mathrm{k}^{+}} \frac{1}{\sqrt{N}} \sum_{j=2,3} \sqrt{\sum_{i=1}^{N} ((\left[\mathbf{s}_\mathrm{k}^{+}\right] + \mathbf{I})^{-1} \mathbf{f}_{m,i}^{\mathrm{ft_k},-} \cdot \mathbf{e}_j)^2} + \mathrm{std}_{i=1,\cdots,N}((\left[\mathbf{s}_\mathrm{k}^{+}\right] + \mathbf{I})^{-1} \mathbf{f}_{m,i}^{\mathrm{ft_k},-} \cdot \mathbf{e}_1)$$

where, $\mathbf{e}_j$ with $j = 1, 2, 3$ are unit vectors in $\mathbb{R}^3$. We estimated the gravity of the leg by

$$m_k g = 1/N \sum_{i=1}^{N} ((\left[\mathbf{s}_\mathrm{k}^{+,*}\right] + \mathbf{I})^{-1} \tilde{\mathbf{f}}_{m,i}^{\mathrm{ft_k}} \cdot \mathbf{e}_1)$$

3) Leg CoM, $\mathrm{r}_k(\phi)$*:* Next, we solved for the leg CoM by subtracting eqn. 6 and eqn. 7.

$$\frac{(6)-(7)}{2}: \quad \begin{aligned} \boldsymbol{\tau}_{m,i}^{\mathrm{ft_k},-} &= [\mathbf{r}_\mathrm{k}(\phi_i)]\,(\left[\mathbf{s}_\mathrm{k}^{+}\right] + \mathbf{I}) m_\mathrm{k} \mathbf{g}_x + \boldsymbol{\omega}_i^{-} \\ &= [\mathbf{r}_\mathrm{k}(\phi_i)]\,\mathbf{f}_{m,i}^{\mathrm{ft_k},-} + \boldsymbol{\omega}_i^{-} \end{aligned}$$

Here $\boldsymbol{\tau}_{m,i}^{\mathrm{ft_k},-}$ and $\mathbf{f}_{m,i}^{\mathrm{ft_k},-}$ could be calculated directly from the measurement data. We estimated the leg CoM $\mathbf{r}_{\text{est,k}}(\phi)$ as a function of ϕ through a Kalman smoother [24], with N samples measured with varying shaft angle ϕ_i, $i = 1, \cdots, N$. We set the transition and observation covariance matrices in the Kalman smoother both having 0.01 on the diagonal and 0 on the off diagonal elements, which matched the magnitude of the measured covariance. Since the torque was the cross product between CoM vector and gravity, the estimated CoM here had a one dimensional null space along the direction of $\tilde{\mathbf{f}}_{m,i}^{\mathrm{ft_k}}$. The CoM could be $\mathbf{r}_\mathrm{k}(\phi_i) = \mathbf{r}_{\text{est,k}}(\phi_i) + p_i \cdot \tilde{\mathbf{f}}_{m,i}^{\mathrm{ft_k}}$, for any scalar $p_i \in \mathbb{R}$. Therefore, we needed at least another pair of opposite hanging measurements to get full rank information on $\mathbf{r}_\mathrm{k}(\phi)$. In our experiment, we took measurements with leg gravity aligning with $\pm z$-axis of the transducer frame and performed analogous calculations mentioned above with $\mathbf{g}_z$. We obtained another estimation $\mathbf{r}'_{\text{est,k}}(\phi)$ where $\mathbf{r}_\mathrm{k}(\phi_i) = \mathbf{r}'_{\text{est,k}}(\phi_i) + p'_i \cdot \tilde{\mathbf{f}'}_{m,i}^{\mathrm{ft_k}}$. We solved p_i, p'_i by equating two $\mathbf{r}_\mathrm{k}(\phi)$ obtained from two sets of measurements. It formed an over-determined system with three equations and two unknowns, so we solved for the unknowns p_i, p'_i by ordinary least squares. We averaged those two $\mathbf{r}_\mathrm{k}$ and fit a function with respect to ϕ.

4) Transducer offset, $\mathbf{w}_\mathrm{o}^{ft_k} = [\mathbf{f}_\mathrm{o}^{ft_k}; \boldsymbol{\tau}_\mathrm{o}^{ft_k}]$*:* Then, we solved for transducer torque offset $\boldsymbol{\tau}_o^{\mathrm{ft_k}}$, by adding eqn. 6 and eqn. 7.

$$\frac{(6)+(7)}{2}: \quad \begin{aligned} \boldsymbol{\tau}_{m,i}^{\mathrm{ft_k},+} = [\mathbf{r}_\mathrm{k}(\phi_i)] &\left(\frac{\left[\mathbf{s}_\mathrm{k}^{\downarrow}\right] - \left[\mathbf{s}_\mathrm{k}^{\uparrow}\right]}{2}\right) m_k \mathbf{g}_x \\ &+ \boldsymbol{\tau}_o^{\mathrm{ft_k}} + \frac{\boldsymbol{\omega}_i^{\downarrow} + \boldsymbol{\omega}_i^{\uparrow}}{2} \end{aligned}$$

We denoted the subtraction between two skew symmetric matrices by $\left[\mathbf{s}_\mathrm{k}^{-}\right] = (\left[\mathbf{s}_\mathrm{k}^{\downarrow}\right] - \left[\mathbf{s}_\mathrm{k}^{\uparrow}\right])/2$. In the transducer model in eqn. 1, we assumed the transducer offset was constant. We solved for the optimal value of $\mathbf{s}_\mathrm{k}^{-}$ by minimizing the standard deviation of $\boldsymbol{\tau}_o^{\mathrm{ft_k}}$ over all samples:

$$\mathbf{s}_\mathrm{k}^{-,*} = \arg\min_{\mathbf{s}_\mathrm{k}^{-}} \underset{i=1,\cdots,N}{\mathrm{std}} \left(\boldsymbol{\tau}_{m,i}^{\mathrm{ft_k},+} - [\mathbf{r}_\mathrm{k}(\phi_i)]\,\left[\mathbf{s}_\mathrm{k}^{-}\right] m_\mathrm{k} \mathbf{g}_x\right)$$

Finally, we calculated the force and torque offsets by:

$$\mathbf{f}_o^{\mathrm{ft_k}} = \frac{1}{N} \sum_{i=1}^{N} \left(\frac{\mathbf{f}_{m,i}^{\mathrm{ft_k},\downarrow} + \mathbf{f}_{m,i}^{\mathrm{ft_k},\uparrow}}{2} - \left[\mathbf{s}_\mathrm{k}^{-,*}\right] m_\mathrm{k} \mathbf{g}_x\right)$$

$$\boldsymbol{\tau}_o^{\mathrm{ft_k}} = \frac{1}{N} \sum_{i=1}^{N} \left(\boldsymbol{\tau}_{m,i}^{\mathrm{ft_k},+} - [\mathbf{r}_\mathrm{k}(\phi_i)]\,\left[\mathbf{s}_\mathrm{k}^{-,*}\right] m_\mathrm{k} \mathbf{g}_x\right)$$

B. Transformation error, $\mathbf{T}_\mathrm{B}^\mathrm{C} \tilde{\mathbf{T}}_\mathrm{k}$

In the second part, we showed our method in estimating the transformation error from transducer frame to body frame,

$$
\begin{aligned}
\mathbf{w}^{\mathsf{W}}_{\text{total},p} &= \sum_{k=1}^{K} [\mathsf{Ad}_{(\mathbf{T}^{\mathsf{W}}_{\mathsf{C},p})^{-1}}]^T \mathbf{w}^{\mathsf{C}}_{\text{gc},k}(\phi_{p,\mathrm{k}}, \mathbf{g}^{\mathsf{C}}_p) \\
\text{(substitute } \mathbf{w}^{\mathsf{C}}_{\text{gc},k} \text{ by eqn.3)} \quad &= \sum_{k=1}^{K} [\mathsf{Ad}_{(\mathbf{T}^{\mathsf{W}}_{\mathsf{C},p})^{-1}}]^T \left(\mathsf{Ad}_{(\mathbf{T}^{\mathsf{C}}_{\mathsf{B}} \tilde{\mathbf{T}}_k \mathbf{T}^{\mathsf{B}}_{\mathrm{ft_k}})^{-1}}]^T (\mathbf{w}^{\mathrm{ft_k}}_{m,p} - \mathbf{w}^{\mathrm{ft_k}}_{o}) - [m_k \mathbf{g}^{\mathsf{C}}_p; \mathbf{T}^{\mathsf{C}}_{\mathsf{B}} \tilde{\mathbf{T}}_k \mathbf{T}^{\mathsf{B}}_{\mathrm{ft_k}} \mathbf{r}^{\mathrm{ft_k}}_{\mathrm{k}}(\phi_{p,\mathrm{k}}) \times m_k \mathbf{g}^{\mathsf{C}}_p] \right) \\
\text{(Expand } \mathbf{T}^{\mathsf{C}}_{\mathsf{B}} \tilde{T}_k) \quad &= \sum_{k=1}^{K} \Bigg(\begin{bmatrix} \mathbf{R}^{\mathsf{W}}_{\mathsf{C}} & \mathbf{0} \\ \mathbf{0} & \mathbf{R}^{\mathsf{W}}_{\mathsf{C}} \end{bmatrix} \begin{bmatrix} \tilde{\mathbf{R}}_k & \mathbf{0} \\ \tilde{\mathbf{R}}_{\mathrm{k}} \left[\tilde{\mathbf{R}}_k (\tilde{\mathbf{p}}_{\mathrm{k}} + \mathbf{p}^{\mathsf{C}}_{\mathsf{B}}) \right] & \tilde{\mathbf{R}}_{\mathrm{k}} \end{bmatrix} [\mathsf{Ad}_{(\mathbf{T}^{\mathsf{B}}_{\mathrm{ft_k}})^{-1}}]^T (\mathbf{w}^{\mathrm{ft_k}}_{m,p} - \mathbf{w}^{\mathrm{ft_k}}_{o}) \\
&\quad - [m_k \mathbf{g}; \begin{bmatrix} \mathbf{R}^{\mathsf{W}}_{\mathsf{C}} & \mathbf{0} \\ \mathbf{0} & 1 \end{bmatrix} \begin{bmatrix} \tilde{\mathbf{R}}_k & \tilde{\mathbf{p}}_{\mathrm{k}} + \mathbf{p}^{\mathsf{C}}_{\mathsf{B}} \\ \mathbf{0} & 1 \end{bmatrix} \mathbf{T}^{\mathsf{B}}_{\mathrm{ft_k}} \mathbf{r}^{\mathrm{ft_k}}_{\mathrm{k}}(\phi_{p,\mathrm{k}}) \times m_k \mathbf{g}] \Bigg) \\
&\approx [0, 0, G_{\text{robot}}, 0, 0, 0]^T
\end{aligned} \tag{9}
$$

$\tilde{\mathbf{T}}_{\mathrm{k}}$ modeled by $(\tilde{\mathbf{R}}_{\mathrm{k}}, \tilde{\mathbf{p}}_{\mathrm{k}})$, together with an unknown transformation between body frame and CoM frame $\mathbf{T}^{\mathsf{C}}_{\mathsf{B}}$ modeled by $(\mathbf{I}_3, p^{\mathsf{C}}_{\mathsf{B}})$. We used the fact that the robot should be at force-torque balance when standing still at different poses. At each pose, the sum of the ground contact wrenches from all feet, transformed to the floating base frame, should equal to the gravity of the robot with zero torque, as calculated in eqn. 9. We used exactly the same dataset as described in §I-B, and inferred the unknown parameters by minimizing the error between the total ground contact wrenches and the gravity of the robot with zero torque, as shown in eqn. 8. It minimized the difference between the measured and expected total wrench on CoM over all $p = 1, \cdots, P$ poses. The K-norm we used had a positive definite diagonal matrix $\mathbf{K}$ to allow us to compare loss functions computed over force and torque, which had different physical units. In practice, we used $1, 1, 1, 10, 10, 10$ in the diagonal elements and zeros elsewhere as the $\mathbf{K}$-norm, so the forces and torques had about the same magnitude.

$$
\min_{\tilde{\mathbf{R}}_{\mathrm{k}}, \tilde{\mathbf{p}}_{\mathrm{k}}, \mathbf{p}^{\mathsf{C}}_{\mathsf{B}}} \sum_{p=1}^{P} ||(\mathbf{w}^{\mathsf{W}}_{\text{total},p} - [0, 0, G_{\text{robot}}, 0, 0, 0]^T)||^2_{\mathbf{K}} \tag{8}
$$

$$
\text{s.t. } \tilde{\mathbf{R}}_k \in SO(3)
$$

This optimization problem needed to constrain the six rotation matrices $\tilde{\mathbf{R}}_{\mathrm{k}}$ onto $SO(3)$ group, which is not a vector space. Most numerical optimization paradigms only work on vector spaces. Instead, we parameterized the rotation using Cayley transformation: $\tilde{\mathbf{R}}_{\mathrm{k}} = (\mathbf{I} - [\tilde{\mathbf{q}}_{\mathrm{k}}])(\mathbf{I} + [\tilde{\mathbf{q}}_{\mathrm{k}}])^{-1}$ [25]. It could represent rotation matrices in a wide range, and the resulted parameter space became a vector space instead of $SO(3)$ group.

In practice, we made a change of variable for $\tilde{\mathbf{p}}'_k = \tilde{\mathbf{R}}_k(\tilde{\mathbf{p}}_k + \mathbf{p}^{\mathsf{C}}_{\mathsf{B}})$. Then the objective function of optimization eqn. 8 had a bilinear form in $\tilde{\mathbf{p}}'_k$ and $\tilde{\mathbf{R}}_{\mathrm{k}}$. We did dual least square optimizations alternatively, fixing one unknown at each step, until it converges. We again used `scipy.optimize.least_squares` Trust Region Reflective algorithm and cost function tolerance 10^{-3}. The dual optimization was considered to be converged, when the maximum norm difference between two successive optimal solutions was less than 10^{-3}.

IV. Results

In this section, we reported the estimated calibration parameters and the residual after calibration. We used violin plots to show the distribution of the residuals, and all violin plots in the paper used 100 points for the Gaussian kernel density estimation.

1) Transducer offset and leg gravity offset: The estimated transducer offset and the leg gravity were summarized in Appendix. We plotted the estimated leg CoM trajectories on the mid-left leg in figure 4 as an example. All the other legs all had similar trajectories, as shown in Appendix. After removing the transducer offsets and the leg gravity offsets, we plotted of the residual of all four orientations in figure 5. We compared our formulation with the naive addition and subtraction, without the axis misalignment error $\hat{\mathbf{s}}$.

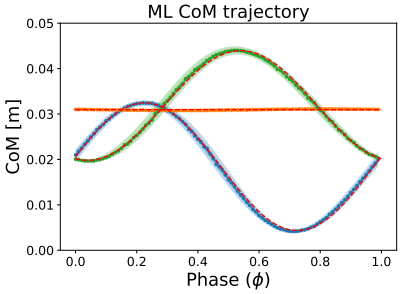

Fig. 4: Estimated center of mass (CoM) vs. phase of Mid-left(ML) leg. We plotted the median estimated CoM of ten cycles in dots, interquartile range in dark shaded region and 95% confidence interval in shallow shaded region (x coordinate in blue, y coordinate in orange and z coordinate in green). We fitted x, z coordinate with function $r(\phi) = A\sin(2\pi\phi + C) + D$, y coordinate using a constant, and plotted them in red dashes.

TABLE I: Summary of model selection statistics. (Abbreviations: degree of freedom(DOF), cross-validation(CV), Bayesian information criterion(BIC)

Model	DOF	CV error	BIC
Full (Six rotations + six translations)	18+18	12	1580
Six rotations + single translation	18+3	17	1674
Six translations only	18	62	2352
Single translation	3	105	2546

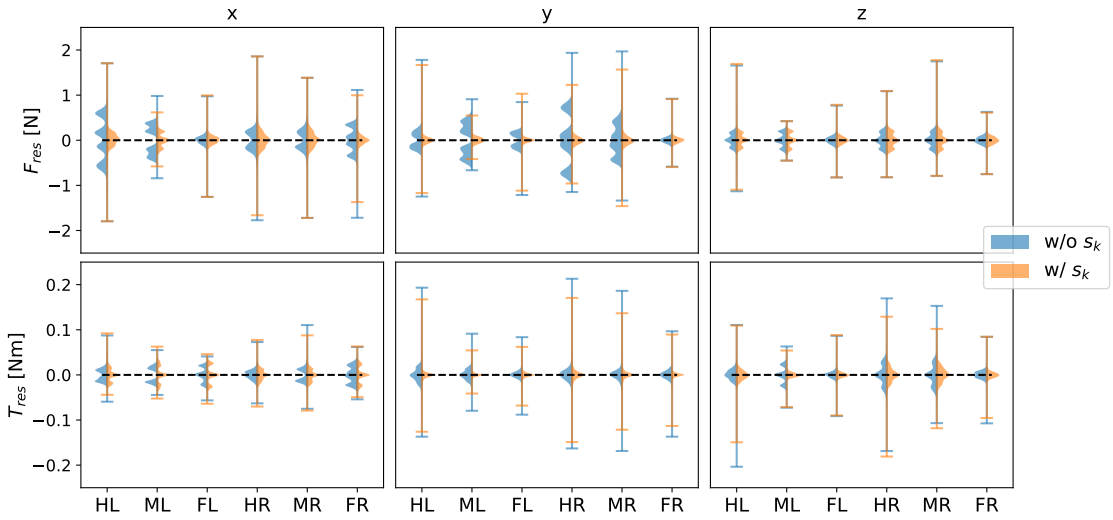

Fig. 5: Violin plot of force (first row) and torque (second row) residual on xyz-axis (columns) for all six transducers. With skew symmetric matrices $\hat{\mathbf{s}}$ accounting for hanging orientation error (orange), without (blue). (FL: front left, ML: mid left, HL: hind left, FR: front right, MR: mid right, HR: hind right).

2) Statistical analysis on wrench transformation error: We performed a model selection on 4 different models, to see the significance of the parameters used to model the wrench transformation error. We tested on

1) The full model, fitting all six rotations ($\tilde{\mathbf{R}}_k$) and six translations ($\tilde{\mathbf{p}}'_k$), using $6 \times (3+3) = 36$ parameters;
2) No transducer translation error ($\tilde{\mathbf{p}}_k = \mathbf{0}$) , only fitting six rotations ($\tilde{\mathbf{R}}_k$) and one single unknown translation ($\mathbf{p}_{\mathrm{B}}^{\mathrm{C}}$) between robot center and CoM, using $6 \times 3 + 3 = 21$ parameters;
3) No transducer rotation error ($\tilde{\mathbf{R}}_k = \mathbf{I}_3$), only fitting the transducer translation error together with robot center to CoM translation ($\tilde{\mathbf{p}}'_k$), using $6 \times 3 = 18$ parameters;
4) With neither transducer rotation, nor translation error, only fitting a single unknown translation between robot center and CoM, using 3 parameters.

The statistics of those models were summarized in table I. We reported mean of the testing mean squared error (MSE) of 5-fold cross validation, together with Bayesian information criterion $\mathrm{BIC} = P \ln(\mathrm{RSS}/P) + \mathrm{DOF} \times \ln P$, where RSS is the residual sum squared. We selected (1) full model using six rotations and six translations, which yielded the smallest BIC. We showed the residual plot comparing with and without transformation errors in figure 6.

3) Tripod walking: We also collected the wrench and motion tracking data when the BigAnt robot used tripod gait to walk quasi-statically. The gait was governed by a Buehler clock running at frequency 0.08Hz and turned right at 9.08^o per gait cycle on average. A more detailed description of the gait can be found in [14], [19]. The measurements compared between naive bias taring and our calibration was attached in the Appendix.

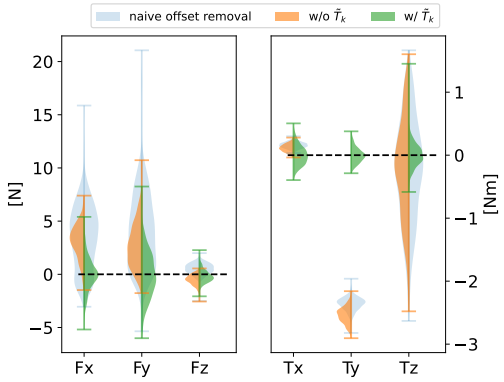

Fig. 6: Violin plot of the residual of the sum of force (left) and torque (right) at robot CoM in floating base frame at different poses. Naive bias removal (light blue), without characterizing transformation error (orange), our calibration method with $(\tilde{\mathbf{R}}_k, \tilde{\mathbf{p}}'_k)$ (green).

V. Conclusions and Discussions

In this paper, we showed the measurements from the six axis f/t transducers on multilegged robots were not accurate, when using them naively. When the robot standing at different poses, the sum of total wrench was far from robot gravity with zero torque at the robot CoM, especially in the planar forces. That poor accuracy on ground contact wrench measurement hindered us from studying the modeling of multi-legged robots.

Herein, we proposed an in-situ calibration framework, to get accurate measurements. We characterized transducer offset, leg gravity offset and the wrench transformation error in our model. We first estimated transducer offset and leg gravity offset by hanging the robot in two set of opposite directions.

Our calibration method took into account of the hanging orientation error $\hat{\mathbf{s}}$, when solving for the transducer offset and tool gravitational offset. The residual had clearly multi-modal distribution in figure 5 without $\hat{\mathbf{s}}$, especially in Fx and Fy. By characterizing an infinitesimal rotation error $\hat{\mathbf{s}}$ during the hanging experiment, the error distribution became more similar to a zero mean normal distribution, with a maximum 0.2N standard deviation. In the second calibration step, we characterized the frame transformation estimation error between transducer frame and body frame, together with the unknown translation between body frame origin and CoM. The unknown translation between body frame origin and CoM removed the 2.5Nm bias in torque estimation. By characterizing the frame transformation estimation error, the 5-fold cross validation residual was improved by 8 times compared with only fitting a single translation transformed to CoM. Therefore, we concluded that this calibration framework enabled us to make much more accurate measurements for the future work in studying legged locomotion mechanism.

We also noticed that the offset term on the transducer could change. Our experience showed the offset changed up to 10N after six months. When a significant offset change happened, while all the parts of the robot remained the same, the offset $\mathbf{w}_o^{\mathrm{ft_k}}$ could be easily re-estimated by putting it as the optimization variables in eqn. 8, with the other calibration parameters remained the same as previous. In this case, the experimenter only need to collect a few extra measurements with robot standing at different poses, without needing to redo the entire hanging experiments.

REFERENCES

[1] M. Y. Cao, S. Laws, and F. R. y. Baena, "Six-axis force/torque sensors for robotics applications: A review," *IEEE Sensors Journal*, vol. 21, no. 24, pp. 27 238–27 251, 2021.

[2] W. Schwalb, B. Shirinzadeh, and J. Smith, "A force-sensing surgical tool with a proximally located force/torque sensor," *The International Journal of Medical Robotics and Computer Assisted Surgery*, vol. 13, no. 1, p. e1737, 2017.

[3] B. Shimano and B. Roth, "On force sensing information and its use in controlling manipulators," *IFAC Proceedings Volumes*, vol. 10, no. 11, pp. 119–126, 1977, iFAC International Symposium on Information-Control Problems in Manufacturing Technology, Tokyo, Japan, 17-20 October.

[4] R. D. Howe, "Tactile sensing and control of robotic manipulation," *Advanced Robotics*, vol. 8, no. 3, pp. 245–261, 1993.

[5] M. Hutter, C. Gehring, A. Lauber, F. Gunther, C. D. Bellicoso, V. Tsounis, P. Fankhauser, R. Diethelm, S. Bachmann, M. Bloesch, H. Kolvenbach, M. Bjelonic, L. Isler, and K. Meyer, "Anymal - toward legged robots for harsh environments," *Advanced Robotics*, vol. 31, no. 17, pp. 918–931, 2017.

[6] H. Komsuolu, K. Sohn, R. J. Full, and D. E. Koditschek, "A physical model for dynamical arthropod running on level ground," in *Experimental Robotics*, O. Khatib, V. Kumar, and G. J. Pappas, Eds. Berlin, Heidelberg: Springer Berlin Heidelberg, 2009, pp. 303–317.

[7] X. A. Wu, T. M. Huh, R. Mukherjee, and M. Cutkosky, "Integrated ground reaction force sensing and terrain classification for small legged robots," *IEEE Robotics and Automation Letters*, vol. 1, no. 2, pp. 1125–1132, 2016.

[8] P.-C. Lin, H. Komsuoglu, and D. Koditschek, "A leg configuration measurement system for full-body pose estimates in a hexapod robot," *IEEE Transactions on Robotics*, vol. 21, no. 3, pp. 411–422, 2005.

[9] J.-H. Kim, "Multi-axis force-torque sensors for measuring zero-moment point in humanoid robots: A review," *IEEE Sensors Journal*, vol. 20, no. 3, pp. 1126–1141, 2020.

[10] U. Saranli, M. Buehler, and D. E. Koditschek, "Rhex: A simple and highly mobile hexapod robot," *The International Journal of Robotics Research*, vol. 20, no. 7, pp. 616–631, 2001.

[11] I. Fitzner, Y. Sun, V. Sachdeva, and S. Revzen, "Rapidly prototyping robots: Using plates and reinforced flexures," *IEEE Robotics & Automation Magazine*, vol. 24, no. 1, pp. 41–47, 2017.

[12] S. Sponberg and R. J. Full, "Neuromechanical response of musculoskeletal structures in cockroaches during rapid running on rough terrain," *Journal of Experimental Biology*, vol. 211, no. 3, pp. 433–446, 02 2008. [Online]. Available: https://doi.org/10.1242/jeb.012385

[13] S. Revzen, S. A. Burden, T. Y. Moore, J.-M. Mongeau, and R. J. Full, "Instantaneous kinematic phase reflects neuromechanical response to lateral perturbations of running cockroaches," *Biological Cybernetics*, vol. 107, no. 2, pp. 179–200, Apr 2013. [Online]. Available: https://doi.org/10.1007/s00422-012-0545-z

[14] D. Zhao and S. Revzen, "Multi-legged steering and slipping with low DoF hexapod robots," *Bioinspiration & Biomimetics*, vol. 15, no. 4, p. 045001, may 2020. [Online]. Available: https://doi.org/10.1088/1748-3190/ab84c0

[15] D. Zhao, B. Bittner, G. Clifton, N. Gravish, and S. Revzen, "Walking is like slithering: A unifying, data-driven view of locomotion," *Proceedings of the National Academy of Sciences*, vol. 119, no. 37, p. e2113222119, 2022. [Online]. Available: https://www.pnas.org/doi/abs/10.1073/pnas.2113222119

[16] C.-J. Kao, C.-S. Chen, and P.-C. Lin, "Reactive force analysis and modulation of the individual legs in a running hexapod robot," in *2019 IEEE/ASME International Conference on Advanced Intelligent Mechatronics (AIM)*, 2019, pp. 370–375.

[17] F. J. A. Chavez, S. Traversaro, D. Pucci, and F. Nori, "Model based in situ calibration of six axis force torque sensors," in *2016 IEEE-RAS 16th International Conference on Humanoid Robots (Humanoids)*, 2016, pp. 422–427.

[18] D. Miller, I. Fitzner, S. Fuller, and S. Revzen, "Focused modularity: Rapid iteration of design and fabrication of a meter-scale hexapedal robot," in *Assistive Robotics: Proceedings of the 18th International Conference on CLAWAR 2015*, 2015, pp. 430–438.

[19] D. Zhao, "Locomotion of low-dof multi-legged robots," Ph.D. dissertation, University of Michigan, 2021.

[20] *F/T Transducer SixAxis Force/Torque Sensor System Installation and Operation Manual*, ATI Industrial Automation, Apex, NC: USA, 2021. [Online]. Available: ati-ia.com/app_content/documents/9620-05-Transducer%20Section.pdf

[21] S. Traversaro, D. Pucci, and F. Nori, "In situ calibration of six-axis force-torque sensors using accelerometer measurements," in *2015 IEEE International Conference on Robotics and Automation (ICRA)*, 2015, pp. 2111–2116.

[22] C. Ding, Y. Han, W. Du, J. Wu, and Z. Xiong, "In situ calibration of six-axis forcetorque sensors for industrial robots with tilting base," *IEEE Transactions on Robotics*, pp. 1–14, 2021.

[23] Y. Yu, R. Shi, and Y. Lou, "Bias estimation and gravity compensation for wrist-mounted force/torque sensor," *IEEE Sensors Journal*, pp. 1–1, 2021.

[24] S. Thrun, W. Burgard, and D. Fox, *Probabilistic Robotics (Intelligent Robotics and Autonomous Agents)*. The MIT Press, 2005, section 3.

[25] R. Courant and D. Hilbert, *Methods of mathematical physics*. Interscience publishers, INC., New York, 1937, vol. 1, section VII.§7.2.

ACKNOWLEDGMENTS

APPENDIX

TABLE II: Summary of the estimated force/torque offsets and the estimated gravity of legs. The top row is the abbreviation of the transducer underneath which leg. (FL: front left, ML: mid left, HL: hind left, FR: front right, MR: mid right, HR: hind right)

	HL	ML	FL	HR	MR	FR
$\mathbf{F}_{\text{offset}}[N]$	1.47 ± 0.03	1.419 ± 0.001	0.57 ± 0.01	-8.49 ± 0.02	-0.06 ± 0.02	-0.93 ± 0.01
	-1.30 ± 0.01	-4.884 ± 0.001	3.71 ± 0.01	-1.448 ± 0.004	-0.123 ± 0.001	0.653 ± 0.001
	-5.61 ± 0.01	-0.406 ± 0.001	-2.039 ± 0.003	-2.43 ± 0.01	-0.07 ± 0.01	-2.183 ± 0.004
$\mathbf{T}_{\text{offset}}[Nm]$	0.2457 ± 0.0002	-0.0136 ± 0.0002	0.2176 ± 0.0001	-0.3159 ± 0.0002	-0.2392 ± 0.0009	-0.3611 ± 0.0004
	0.002 ± 0.003	0.0808 ± 0.0002	0.0921 ± 0.0005	0.3449 ± 0.0009	-0.0982 ± 0.0012	-0.153 ± 0.001
	0.034 ± 0.003	0.0144 ± 0.0001	-0.0177 ± 0.0004	0.001 ± 0.001	0.004 ± 0.001	0.0222 ± 0.0007
$mg[N]$	6.2 ± 0.2	6.2 ± 0.2	6.2 ± 0.1	6.1 ± 0.2	6.2 ± 0.2	6.4 ± 0.1

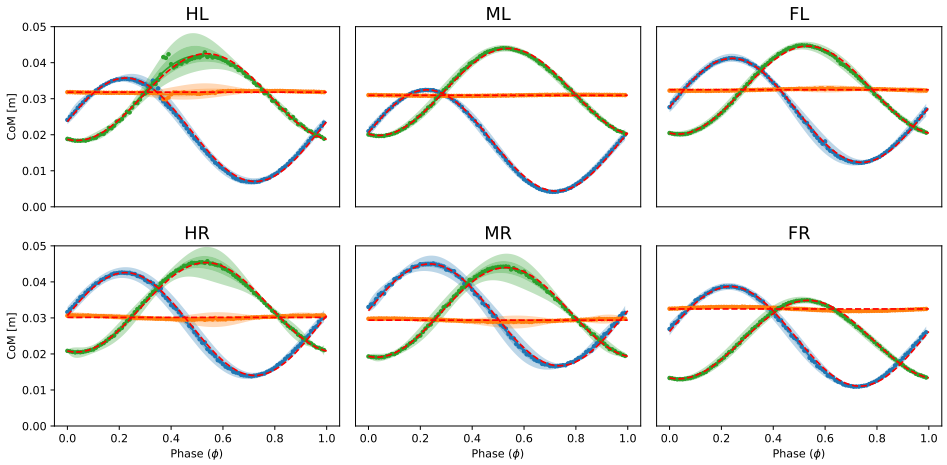

Fig. 7: Estimated center of mass (CoM) vs. phase of all six legs. We plotted the median estimated CoM of ten cycles in dots, interquartile range in dark shaded region and 95% confidence interval in shallow shaded region (x coordinate in blue, y coordinate in orange and z coordinate in green). We fitted x, z coordinate with function $r(\phi) = A\sin(2\pi\phi + C) + D$, y coordinate using a constant, and plotted them in red dashes.

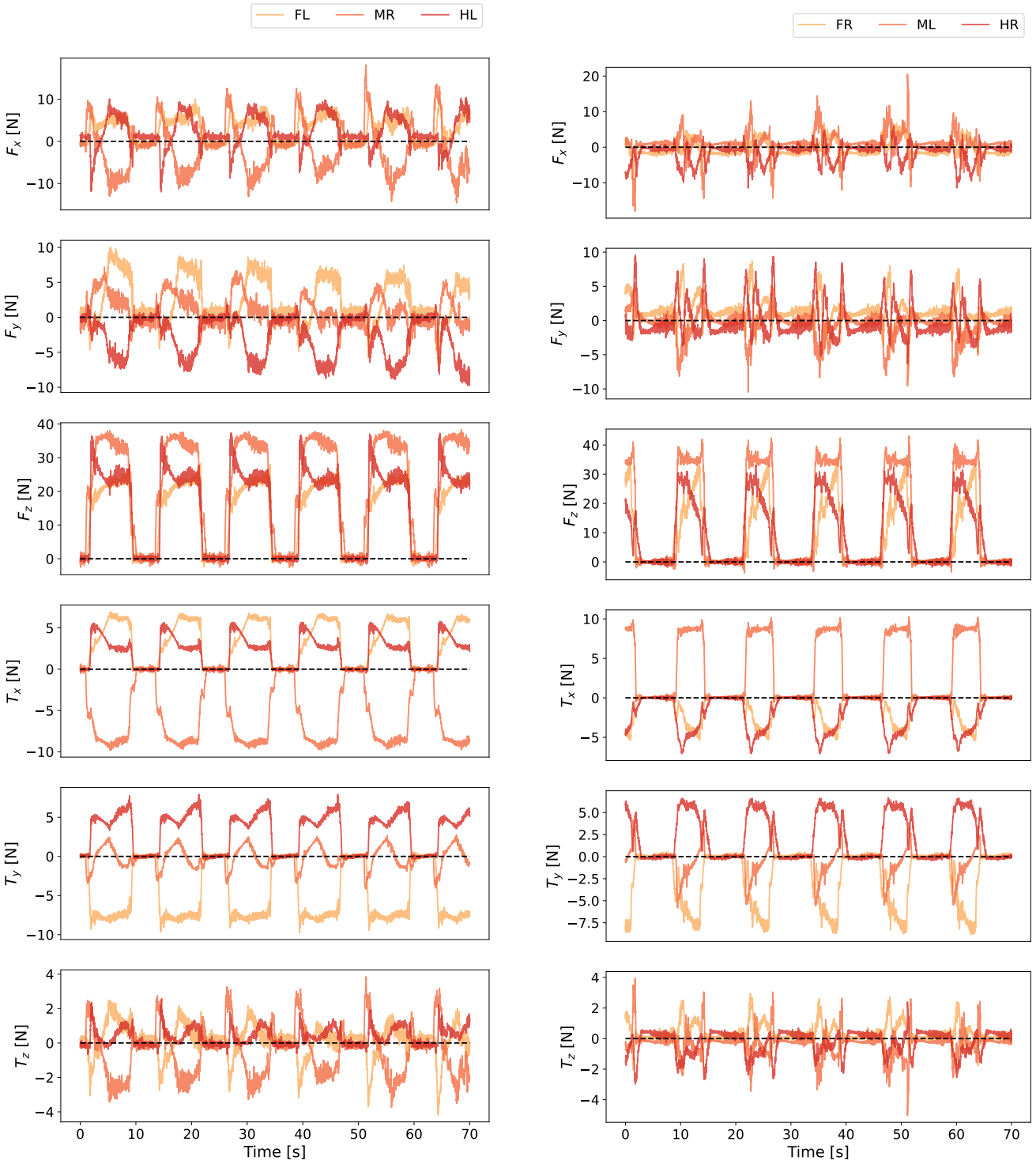

(a) Left tripod.(FL: front left, MR: mid right, HL: hind left)

(b) Right tripod.(FR: front right, ML: mid left, HR: hind right)

Fig. 8: All groud contact wrenches measured from the f/t transducers with naive taring transformed to the floating base frame. (FL: front left, ML: mid left, HL: hind left, FR: front right, MR: mid right, HR: hind right)

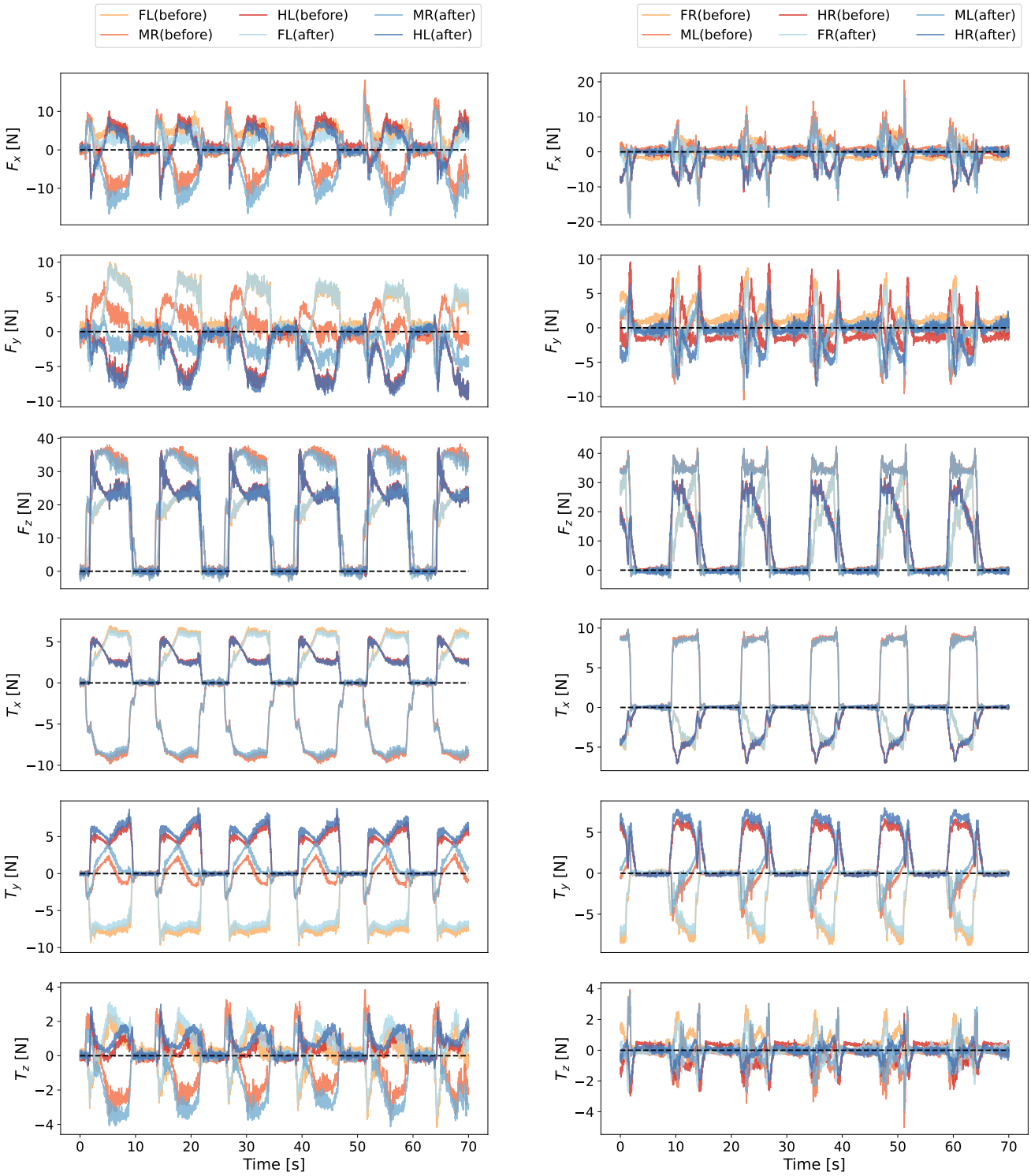

(a) Left tripod.(FL: front left, MR: mid right, HL: hind left)

(b) Right tripod.(FR: front right, ML: mid left, HR: hind right)

Fig. 9: All groud contact wrenches at the floating base frame after calibration compared with with naive taring.